

## Effect of kind of acid and the solid fraction on the viscosity by the $\gamma$ -Al<sub>2</sub>O<sub>3</sub> nanofiber in the form of precursor slurry for the final ceramic

Adrián Zamorategui<sup>a,\*</sup>, Oscar Coreño<sup>a</sup>, Julio Del Angel<sup>b</sup> and Satoshi Tanaka<sup>c</sup>

<sup>a</sup>Department of Civil Engineering, University of Guanajuato, Guanajuato, Gto., Mexico. Av. Juárez 77, Center; CP 36000

<sup>b</sup>Department of Chemistry, University of Guanajuato, Guanajuato, Gto., Mexico

<sup>c</sup>Department of Materials Science and Technology, Nagaoka University of Technology 1603-1Kamitomioka, Nagaoka, Japan 940-2188

Nanofibers of gamma alumina were dispersed in acid aqueous media and the effect of hydrochloric and nitric acid on viscosity was investigated. The viscosities of the aqueous suspensions were determined under controlled shear rate conditions, varying the pH and solid concentration. A lower viscosity is observed with nitric acid because the nitrate ion produces stronger double layer repulsion, in comparison with that obtained with the chloride ion. It was found that the maximum solid loading in the suspension at pH 4.5 adjusted with HNO<sub>3</sub> and HCl was 42 and 35 wt%, respectively. The isoelectric point (IEP) of the alumina powder in the suspension occurs at pH 8.5. High solid concentrations and a pH close to the IEP produced high viscosity and shear thinning at the low shear rates due to slurry agglomeration. This increases the viscosity of the suspension and diminishes the final relative density of the slip casting body.

**Key words:** Gamma alumina, Nanofiber, Viscosity, Solid loading.

### Introduction

Porous materials have been associated mainly with their specific properties, such as high surface area, high permeability, low thermal conductivity, and low mass [1–4]. Recently, considerable attention has been focused towards porous body gamma alumina ( $\gamma$ -Al<sub>2</sub>O<sub>3</sub>) nanostructures due to their widespread application, such as catalyst supports, porous electrodes, gas distributors, membranes, coatings, adsorbents and insulators [5–8]. Aqueous solutions (slurries) must fulfill certain requirements in some methods that are used for shaping ceramic products such as tape casting, gel casting, slip casting or spray-drying [9–10]. The slurries should have a high solid content and fine particle with homogeneous size distributions and shape to achieve reasonable casting rates. However, nanofibers with high surface area tend to agglomerate due to the high surface energy [11]. Consequently, the particle–particle interactions induce high viscosity and the handling difficulty of the slurry increases [12]. The fabrication of porous bodies is achieved by stacking the particles using aqueous slip casts, and evaluating certain parameters (zeta potential ( $\zeta$ -potential), viscosity, and solid loading) [13, 14].

The stability of a colloidal suspension is related to the  $\zeta$ -potential, which is determined by particle type, suspension formulation, and pH. In order to improve

the quality of the final ceramic it is crucial to evaluate the behavior of the starting materials during processing. These materials must form calibrated slurry with convenient viscosity properties, which depend on pH, solid loading, particle shape, and size [15]. Colloidal suspensions are commonly analyzed by rheological techniques, which are also used as quality control standards, which attempt to minimize the variation in suspensions prior to performing the consolidation procedure, i.e. slip casting, so as to control and optimize the microstructure of the final product [16]. Thus, the suspension requires a source containing the highest particle concentration and lowest viscosity, which depend on the pH and the  $\zeta$ -potential.

The purpose of this study is to evaluate the effects of HCl and HNO<sub>3</sub> and the solid loading on the viscosity of fibrillar  $\gamma$ -Al<sub>2</sub>O<sub>3</sub> suspensions in order to determine the dispersed maximum solids loading.

### Experimental Procedure

The  $\gamma$ -Al<sub>2</sub>O<sub>3</sub> was prepared following the homogeneous precipitation method. Spherical submicron particles of basic aluminum sulfate were synthesized from a mixture of aluminum sulfate and ammonium bisulfite solutions. This basic aluminum sulfate is then neutralized by a solid/liquid reaction with an ammonia solution in order to transform it to aluminum hydroxides. Then, the hydroxides are oven dried at 120 °C to obtain pseudoboehmite ( $\gamma$ -AlOOH), which was used as  $\gamma$ -Al<sub>2</sub>O<sub>3</sub> precursor since it transforms to this phase at 450 °C [17–19].

The morphology and particle size of  $\gamma$ -Al<sub>2</sub>O<sub>3</sub> powders were examined by Field Emission Scanning

\*Corresponding author:

Tel : +52(01)-473-102-01-00 Ext. 2245

Fax: +52(01)-473-102-01-00 Ext.2230

E-mail: zamorategui@ugto.mx

Electron Microscopy (FE-SEM; JEOL JSM 7401F) and Transmission Electron Microscopy (TEM; Phillips Tecnai F-20 Field Emission Microscope). The specific surface area was measured by single-point BET measurements (ASAP 2010 Micromeritics Instrument Corp., USA). The variation of the  $\zeta$ -potential was measured using a 10 mM solution of KCl by the electroacoustic technique with a particle size analyzer (AcoustoSizer II, ESA; Colloidal Dynamics, USA). The viscosities of the dispersions were evaluated using an AR2000 rheometer (AR-2000, TA Instruments) at 25 °C.

Dispersions of  $\gamma$ -Al<sub>2</sub>O<sub>3</sub> nanofibers were prepared using 10, 15, 20, 25, 30 and 35 wt% and introduced into an attrition mill where they were milled for 8 hours using 90 g of 2 mm zirconia beads. Analytical grade hydrochloric and nitric acid were added to adjust the acid pH, and ammonium hydroxide was used to shift the basic pH of the slurry. Then, the samples were slip cast in 25 mm diameter cylindrical rubber molds, allowing the green bodies obtained to dry under atmospheric conditions and later at 120 °C. The dried specimens were heat treated at temperatures of 450, 600, 900 and 1200 °C. The apparent densities of the heat-treated bodies were measured by the Archimedes Method.

## Results and Discussion

### Powder characterization

The adsorption-desorption isotherm of  $\gamma$ -Al<sub>2</sub>O<sub>3</sub> powder is of type IV according to the IUPAC definition, which is characteristic of a mesoporous material (Fig. 1). The irregularly shaped isotherm, with an H3 type hysteresis loop, indicates that the pores have an inkwell-type shape with non-uniform size. The surface area and pore size distribution obtained by the BET method and BJH adsorption model for the  $\gamma$ -Al<sub>2</sub>O<sub>3</sub> (450 °C) were 333 m<sup>2</sup>/g and 4.7 nm respectively [20-22].

Fig. 2(a) shows the TEM image of the nanofiber  $\gamma$ -Al<sub>2</sub>O<sub>3</sub> prepared by homogeneous precipitation. The TEM image suggests that the fibers are around 80 nm long. As observed by FE-SEM, the nanofibers tend to form amorphous agglomerates due to their high surface energy (Fig. 2(b)) [23]. The high value of energy and surface area is related with the high internal porosity produced by the agglomerate of the nanofiber.

### $\zeta$ -Potential and particle size

Fig. 3 shows the effect of pH variation on the zeta potential and type of acid (HNO<sub>3</sub> and HCl) on the particle size of the  $\gamma$ -Al<sub>2</sub>O<sub>3</sub> powder dispersed in water (15 wt%). The profile of the zeta potential versus pH corresponding to changes in surface charge for particles shows the characteristic shape and isoelectric point (IEP) typical for  $\gamma$ -Al<sub>2</sub>O<sub>3</sub> (pH 8.5) [24]. As can be seen, the  $\zeta$ -potential in the  $\gamma$ -Al<sub>2</sub>O<sub>3</sub> suspension is higher using HNO<sub>3</sub> in comparison with HCl, either below or

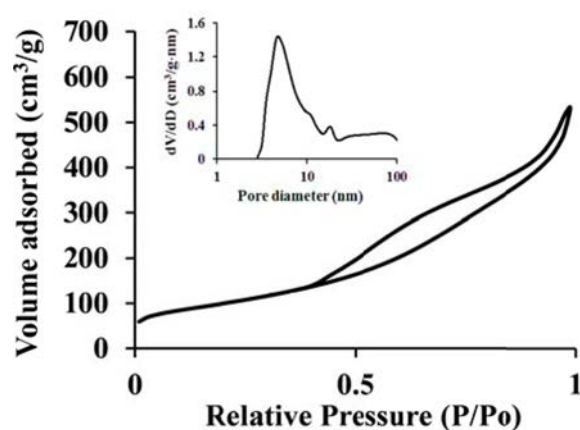


Fig. 1. Nitrogen adsorption-desorption isotherm and pore-size distribution curves of  $\gamma$ -Al<sub>2</sub>O<sub>3</sub>.

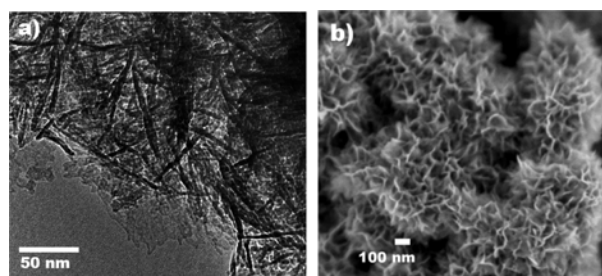


Fig. 2. Micrograph of  $\gamma$ -Al<sub>2</sub>O<sub>3</sub> powder: a) TEM and b) FE-SEM.

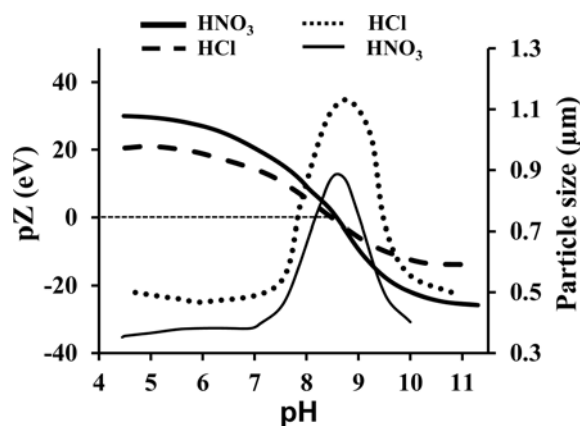
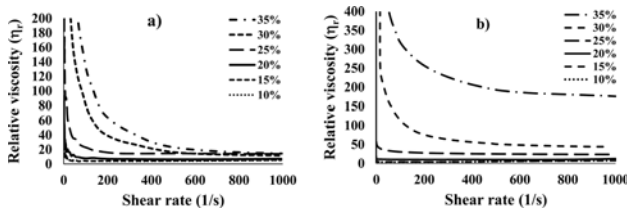


Fig. 3.  $\zeta$ -potential profiles and particle size for the  $\gamma$ -Al<sub>2</sub>O<sub>3</sub> suspension as a function of pH adjusted with HNO<sub>3</sub> and HCl.

above the IEP, i.e., for the particles negatively and positively charged. [25].

As can be seen in figure 3, below pH 7 the suspension has a small particle size, which is in agreement with the high  $\zeta$ -potential measured at these pH values. The particle size drastically increases from pH 7.5, reaching its maximum value at about pH 8.5 (IEP), denoting high flocculation because electrostatic repulsion forces diminish as they become comparable to the inter-particle Van der Waals attractive forces [26]. Finally, the particle size decreases around pH 11 as the particles become increasingly negatively charged generating deflocculation above the IEP, which yields stable suspensions.



**Fig. 4.** Relative viscosity curves of  $\gamma$ -Al<sub>2</sub>O<sub>3</sub> suspensions at pH 4.5 adjusted with: a) HNO<sub>3</sub> and b) HCl and varying the solid loading.

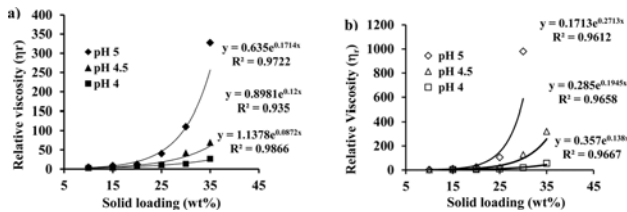


**Fig. 5.** Relative viscosity ( $200 \text{ s}^{-1}$ ) as a function of solid loading at pH 4, 4.5 and 5 adjusted with: a) HNO<sub>3</sub> and b) HCl.

The particle size of the suspension increases slightly using hydrochloric acid in comparison with the nitric acid in all ranges of pH (4 to 12). These acids dissociate a hydronium ion ( $\text{H}_3\text{O}^+$ ) and are chemically bonded to the surface particle, increasing the surface charge by +1 in both cases. However, the double layer formed using HNO<sub>3</sub> can be more extensive because the counter nitrate ion ( $\text{NO}_3^-$ ) larger than the chloride anion ( $\text{Cl}^-$ ) and therefore cannot be compressed as easily. It is widely known that the  $\text{Cl}^-$  anion compresses the double layer more, and the electrostatic repulsion force of dispersed particles is consequently reduced [27-29]. However, the  $\text{NO}_3^-$  ion produces a stronger double layer, and the electrostatic repulsion induces the breakdown of agglomerates into nanoparticles while allowing for diminishing viscosity (Fig. 4).

### Relative viscosity

The relative viscosity of a suspension,  $\eta_r$ , is defined as the ratio of the suspension viscosity,  $\eta_s$ , to the solvent viscosity,  $\eta_0$ : ( $\eta_r/\eta_0$ ) [30]. Fig. 4 shows the relative viscosity variation of  $\gamma$ -Al<sub>2</sub>O<sub>3</sub> suspensions for different solid concentrations, at pH 4.5 adjusted with HNO<sub>3</sub> and HCl. As expected, the relative viscosity increases with the solid concentration because higher resistance to flow is generated by the increasing number of particles per unit volume. Thus, the colloidal suspensions show shear thinning flow behavior at high solid loading above 30 wt% and a low shear rate, where the particles maintain a random distribution [31]. But, the Newtonian behavior is achieved at a low solid loading below 30% and high shear rate, indicating that the particle agglomerates in the suspensions were broken with increased shear rate up to  $150 \text{ s}^{-1}$ , resulting in ordered particle layers.

As shown in Fig. 4(b), the viscosity is much higher using HCl in comparison with that observed in figure 4a for the HNO<sub>3</sub> for the concentrations above 25 wt%. Thus, at the low shear rate in concentrated slurries,

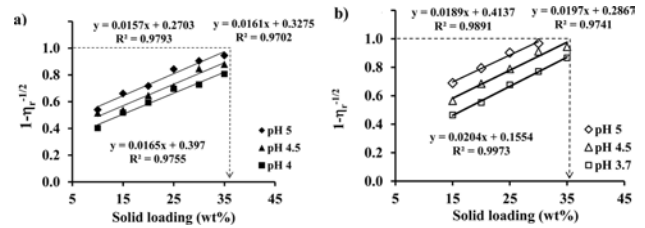


**Fig. 6.**  $(1 - \eta_r^{-1/2})$  versus solid loading for  $\gamma$ -Al<sub>2</sub>O<sub>3</sub> suspension at pH 4, 4.5 and 5 adjusted with: a) HNO<sub>3</sub> and b) HCl.

where the distance between the fibers tends to zero, the viscosity increases due to the great interaction generated by the Brownian motion [32].

Fig. 5 shows the relative viscosity of the suspensions as a function of solid content at a shear rate of  $200 \text{ s}^{-1}$  for the pH 4, 4.5 and 5. Those were adjusted with nitric and hydrochloric acid. At low solid loadings (i.e. up to 15 wt%) the relative viscosity remains low at all pH variations studied. However, for the HCl the relative viscosities of the suspensions start to increase drastically once solid loading reaches 20 wt%. Above 25 wt% the relative viscosity of the suspension at pH 5 rose very sharply, and it does not flow above 35 wt%, in comparison with the HNO<sub>3</sub> (35 wt%). Consequently, the viscosity increases exponentially with the solid loading. For suspensions at pH 4.5, the rate of increase is much slower according to its zeta potential. Additionally, the viscosity of the dispersions of the  $\gamma$ -Al<sub>2</sub>O<sub>3</sub> increased much more with HCl than those observed with HNO<sub>3</sub> as shown in Fig. 5(b) and Fig. 5(a) respectively. This can be due to the better effect of the HNO<sub>3</sub> as a peptizing agent. Thus, both the type of acid used and the pH affect the viscosity drastically, which is used to determine the maximum solid loading, related to the particle concentration for which the viscosity become infinite.

### Maximum solid concentration

The viscosity approaches infinity at a maximum solid concentration ( $\phi_m$ ) in wt% at which the average separation distance between the particles tends to zero and the dispersion ceases to flow, due to the resistance arising from increased particle to particle contact in the suspension and the particles packed together. The  $\phi_m$  allowable for powder suspension can be predicted following a viscosity solid concentration relationship proposed by the modified Krieger-Dougherty equation [33-35]:

$$\eta_r = (1 - \phi/\phi_m)^{-n} \quad (1)$$

As shown in Fig. 6, the  $\phi_m$  at which the suspension behaves as a solid can be estimated by extrapolating the fitted straight line to  $(1 - \eta_r^{-1/2}) \rightarrow 1$ , obtaining a  $\phi_m = 42$  and 35 wt% (Volumetric solid fraction 0.183 and 0.153 respectively) at pH 4.5 adjusted with HNO<sub>3</sub> and HCl respectively. The large difference between the  $\phi_m$

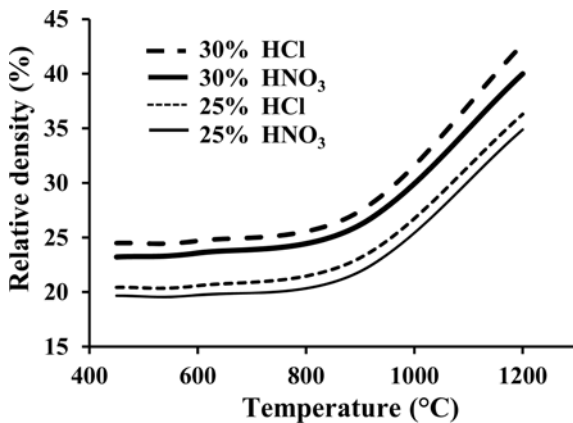


Fig. 7. Relative densities (%) of the porous bodies as a function of solid loading and heat treatment.

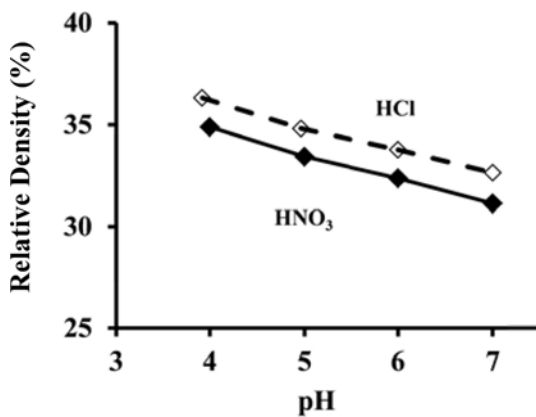


Fig. 8. Effect of pH on the relative density of the heat treated (1200 °C) produced by slip casting (25 wt%).

and that of the random close packing (Maximum volumetric solid fraction  $\sim 0.64$ ) may provide a measure of the dominant attractive forces, considered important to the porosity reached as a function of the pH.

### Relative density of porous bodies

Fig. 7 shows the effect of heating temperature in the relative density of the heat-treated bodies produced by slip casting. The green bodies from suspensions of 25 and 30 wt% were prepared at pH 4.5. After heat treatment at 450, 600, 900 and 1200 °C for one hour, the density was measured. In all cases, the relative density seems to remain constant from 450 to 900 °C and then drastically increases at the high temperature of 1200 °C. This behavior is attributed to the change of phase developed for  $\gamma$ -Al<sub>2</sub>O<sub>3</sub>, which transforms to theta alumina at around 900°C and finally to alpha alumina at around 1200 °C [36, 37]. Also, the relative density of heated bodies and that were prepared with 25 wt% was significantly lower than that obtained for 30 wt%, which shows the effect of the inter-particle contact in the viscosity. Higher solid loading promotes more particle-particle interactions by reducing the inter-particle space occupied by water and consequently increasing the relative density. Additionally, the heat-

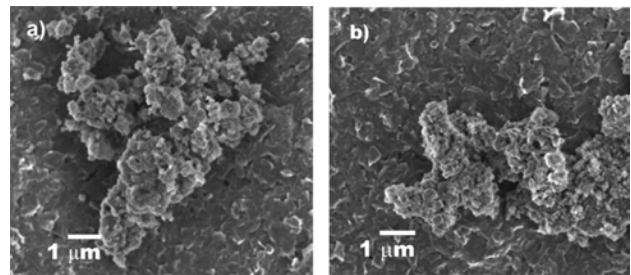


Fig. 9. FE-SEM micrographs of porous bodies prepared by slip cast (25 wt%), pH 4.5 adjusted with: a) HNO<sub>3</sub> and b) HCl.

treated bodies prepared with nitric acid have lower relative density than that observed using hydrochloric acid. This can be attributable to the shrinkage effect during the drying process of the green body. The higher porosity is generated by the interstitial spaces created by the nitrate ion in coordination with a water molecule. Thus the higher shrinkage of the heat-treated bodies promoted by the chloride ion generates a high density in comparison with that obtained with the nitrate ion.

Fig. 8 shows the effect of pH on the relative density of the heat-treated bodies (1200 °C). The green bodies produced by slip casting (25 wt%) were prepared by varying the pH. After heat-treatment at 1200 °C for 60 min, the density was measured by Archimedes method. The relative density of the heat-treated bodies prepared with HNO<sub>3</sub> always remains lower than that obtained by the HCl and gradually decreases with increasing pH. These results are consistent with the observed effect of pH on  $\zeta$ -potential and the chemical behavior of the counter ion in the aqueous suspensions.

Fig. 9 shows the morphology observed by FE-SEM of the heat-treated bodies at 900 °C. Soft spheroidal agglomerates and higher porosity can be observed for the body prepared with HNO<sub>3</sub> (Fig. 9(a)) in comparison with the smaller and more spherical agglomerates conforming a more compact structure for the body prepared with HCl (Fig. 9(b)). Such differences are derived from the chemical behavior of the nitrate and chloride ion used as a peptizing agent. As it is known, the double layer formed for the HNO<sub>3</sub> can be more extensive because the counter NO<sub>3</sub><sup>-</sup> ion is quite large and the Cl<sup>-</sup> ion compresses the double layer and the electrostatic repulsion force of dispersed particles is consequently reduced. Thus, the NO<sub>3</sub><sup>-</sup> ion produces a stronger double layer and electrostatic repulsion inducing the breakdown of agglomerates.

### Conclusions

The physicochemical behavior of the hydrochloric and nitric acid affect the viscosity of the slurry  $\gamma$ -Al<sub>2</sub>O<sub>3</sub> but the flow behavior is maintained at the same pH. The viscosity increased using HCl due to the effect of the chloride ion that compress the electric double layer of the particle in the suspension. Thus, the viscosity

increases in comparison with the low viscosity generated using  $HNO_3$ , which is a better peptizing agent. Thus, the maximum solid loading dispersed at pH 4.5 for easy manipulation of the suspension, using  $HNO_3$  and  $HCl$  were 42 and 35 wt%, respectively. As a result, final density and porosity of porous compact bodies of fiber  $\gamma$ - $Al_2O_3$  were affected by the physicochemical behavior of the nitrate and chloride ion, solid loading and pH. The pH close to the IEP promotes the particle agglomeration and the viscosity increases due to the neutral surface charge of the particle and the low repulsive forces. In concentrated suspensions of fibrous particles the energy dissipation related with its morphology increases the viscosity, making it necessary to adjust the pH in order to obtain Newtonian flow with high solid loading.

### Acknowledgments

We would like to express our gratitude to the *Nagaoka University of Technology 1603-1Kamitomioka, Nagaoka, Japan 940-2188*, for the assistance in the use of the Physica MCR Rheometer.

### References

1. L. Sharifi, S. Ghanbarnazhad, S. Ghofrani and S.H. Mirhosseini, *International Journal of Advanced Science and Technology* 65 (2014) 59-70.
2. T. Isobe, Y. Kameshima, A. Nakajima, K. Okada, *Journal of the European Ceramic Society* 27 (2007) 61-66.
3. S. Deville, E. Saiz, A.P. Tomsia, *Acta Materialia* 55 (2007) 1965-1974.
4. I. Sopyan, C. M. Mardziah, S. Ramesh, *Applied Mechanics and Materials* 117-119 (2012) 827-830.
5. A. Alemi, Z. Hosseinpour, M. Dolatyari, and A. Bakhtiari, *Phys. Status Solidi B*, 249 (2012) 1264-1270.
6. F. Karouia, M. Boualleg, M. Digne, P. Alphonse, *Powder Technology*. 237 (2013) 602-609.
7. C.L. Lu, J.G. Lv, L. Xu, X.F. Guo, W.H. Hou, Y. Hu and H. Huang, *Nanotechnology* 20 (2009) 215604.
8. M.C. Park, S.R. Lee, H. Kim, I. Park, and J.H. Choy, *Bull. Korean Chem. Soc.* 33 (2012) 1962-1966.
9. V. Naglieri, D. Gutknecht, V. Garnier, P. Palmero, *Materials* 6 (2013) 5382-5397.
10. A.R. Studart, U.T. Gonzenbach, E. Tervoort, and L.J. Gauckler, *J. Am. Ceram. Soc.* 89 (2006) 1771-1789.
11. K. Lu, C. Kessler, *J. Mater. Sci.* 41 (2006) 5613-5618.
12. M. Kole, T.K. Dey, *Experimental Thermal and Fluid Science* 34 (2010) 677-683.
13. A. Kritikaki, A. Tsetsekou, *Journal of the European Ceramic Society* 29 (2009) 1603-1611.
14. J.J. Gulicovski, L.S. Cerovic and S.K. Milonjic, *Korea-Australia Rheology Journal* 20 (2008) 65-71.
15. E.J. Teh, Y.K. Leong, Y. Liu, A.B. Fourie, M. Fahey, *Chemical Engineering Science* 64 (2009) 3817-3825.
16. E. Behzadfar, M.H. Abdolrasouli, F. Sharif and H. Nazockdast, *Brazilian Journal of Chemical Engineering* 26 (2009) 713-721.
17. A.C. Vieira Coelho, G.A. Rocha, P. Souza Santos, H. Souza Santos, P.K. Kiyohara, *Revista Matéria* 13 (2008) 329-341.
18. J.R. Vigiúé, B. Sukmanowski, B. Nölting, F.X. Royer, *Eng. Aspects* 302 (2007) 269-275.
19. A. Zamorategui, J.A. Soto, and S. Sugita, *Advances and Applications in Mechanical Engineering and Technology* 4 (2013) 1-17.
20. M. Thommes, *Chemie Ingenieur Technik* 82 (2010) 1059-1073.
21. M.B. Yue, T. Xue, W. Q. Jiao, Y. M. Wang, M.Y. He, *Solid State Sciences* 13 (2011) 409-416.
22. Y.X. Zhang, Y. Jia, Z. Jin, X.Y. Yu, W.H. Xu, T. Luo, B.J. Zhu, J.H. Liu and X.J. Huang, *Cryst. Eng. Comm.* 14 (2012) 3005-3007.
23. A. Zamorategui, S. Sugita, R. Zarraga, S. Tanaka and K. Uematsu, *Journal of the Ceramic Society of Japan* 120 (2012) 290-294.
24. M. Kosmulski, *Journal of Colloid and Interface Science* 275 (2004) 214-224.
25. P.K. Senapati, B.K. Mishra, A. Parida, *Powder Technology* 197 (2010) 1-8.
26. T. Tadros, *Advances in Colloid and Interface Science*. 168 (2011) 263-277.
27. R. Bleta, O. Jaubert, M. Gressier, M.J. Menu, *Journal of Colloid and Interface Science* 363 (2011) 557-565.
28. W. Wunderlich, R.R. Mukti, S. Winardi, K.N.P. Kumar, and T. Okubo, *Proc. School of Eng. Tokai Univ. Ser. E* 34 (2009) 11-16.
29. R. Petrovic, S. Milonjic, V. Jokanovic, L. Kostic-Gvozdenovic, I. Petrovic-Prelevic, D. Janackovic, *Powder Technology* 133 (2003) 185-189.
30. D.B. Genovese, *Advances in Colloid and Interface Science* 171-172 (2012) 1.
31. X. Xu, S.A. Rice, and A.R. Dinner, *PNAS*. 110 (2013) 3771-3776.
32. J. Kaldasch, B. Senge and J. Laven, *Journal of Thermodynamics* 2015 (2014) 1-10.
33. M.J. Santillán, F. Membrives, N. Quaranta and A.R. Boccaccini, *J. Nanoparticle Res.* 10 (2008) 787-793.
34. I.M. Mahbubul, R. Saidur, M.A. Amalina, *International Journal of Heat and Mass Transfer* 55 (2012) 874-885.
35. By S. Mueller, E. W. Llewellyn and H. M. Mader, *Proc. R. Soc. A* 466 (2010) 1201-1228.
36. G.V. Franks, W and Yang Ganz, *J. Am. Ceram. Soc.* 90 (2007) 3373-3388.
37. Y. Deng, Q. Yang, G. Lu, W. Hu, *Ceramics International* 36 (2010) 1773-1777.